Semi-analytic pressure regulated feedback modulated star formation in the Santa Cruz SAM

Austen Gabrielpillai

May 23, 2024

Contents

1 Introduction

Star formation on galactic scales has been a monumental problem to tackle with the increasing breadth and availability of data-rich observations. There have been many attempts to create a global star formation law (Schmidt, 1959; Kennicutt, 1989) that describes galactic star formation for all galaxy types, spanning (but not limited to) disk-dominated spirals, bulge-dominated elliptical, and dwarf irregulars. Not only do attempts at global laws break down for specific galaxy types, but there is need to consider the redshift dependence and evolution of such relationships. There is also uncertainty in measurements of star formation rates (SFRs) to constrain these models due to what gas is used as a star formation tracer or to how far out the gas is measured and resolved in imaging. The problem only grows when considering recent observations from JWST, where galaxies are apparently larger and brighter than previously theorized at high redshifts ($z > 9$). This provides a motive for testing and developing new theoretical models that are able to reproduce both low- and high-redshift observations.

Theoretical modeling of galactic star formation is just as difficult as a problem in observation for similar and different reasons. Although hydrodynamic simulations are capable of resolving single stars on the dwarf galaxy scale, high-resolution cosmological simulations still need the use of sub-grid recipes to calculate the star formation per gas cell and may not be able to resolve disk related structure. Semi-analytic

models also rely on global star formation recipes due to minimal resolution elements, such as tracking galactic disk and bulge sizes. Some star formation frameworks also require the tracking of multiphase gas for HI (neutral hydrogen) and H2 (molecular hydrogen) partitioning. The modeling of such subspecies requires careful treatment of interstellar medium (ISM) cooling and heating, stellar radiative transfer, supernovae feedback energy injection, and more. Thus, there is a need to create a generalized framework that is applicable to a wide population of galaxies that is computationally inexpensive while making as few assumptions as possible. One such method is pressure regulated, feedback modulated (PRFM) star formation (Ostriker & Kim, 2022) where star formation in the galactic disk is dependent on both the disk being in dynamic equilibrium and the coupling of pressure and feedback. This methodology circumvents the need for tracking multiphase gas, is potentially applicable to estimating SFRs globally for galaxy populations, and is redshift-independent.

In this write-up, we present results on applying PRFM, a new, robust model of star formation, in post-processing on a $z = 0$ galaxy catalog produced by a semi-analytic model of galaxy formation. In §2, we outline Santa Cruz semi-analytic model, the base model utilized in this work. §3 we outline the three star formation models that we will compare against: the Kennicutt-Schmidt relation, Gnedin- Kravtsov multiphase partitioning model (fiducial), and pressure regulated, feedback modulated star formation (PRFM). §4 compares the predicted star formation using these models, and lastly we will discuss and summarize the results in §5.

2 Galaxy formation model and catalog

In this section briefly describe the Santa Cruz semi-analytic model of galaxy formation (SC SAM). For a more thorough description, we refer the reader to Somerville *et al.* (2021). The SAM operates on a set of dark matter halo merger trees starting with the lowest level halos, tracking hot circumgalactic gas accretion and cooling into the interstellar medium (ISM), the formation and destruction of stars, chemical enrichment of gas, black hole seeding and growth, as well as mergers and tidal destruction through the tree's timesteps. The specific (in this case, fiducial) star formation model used in the SAM is further elaborated on in Sec. 3.

The simulation catalog used in this work are the $z = 0$ SC SAM runs on IllustrisTNG (Nelson *et al.*, 2018) dark matter-only merger trees identified using the ROCKSTAR halo finder (Behroozi *et al.*, 2013b) and CONSISTENT-TREES merger tree constructor (Behroozi *et al.*, 2013a) codes as detailed in Gabrielpillai *et al.* (2022). For this work, we are specifically using the 50 Mpc volume (Nelson *et al.*, 2019; Pillepich *et al.*, 2019) with a dark matter particle mass resolution of $m_{\rm DM} = M_\odot$ in ΛCDM cosmology: $\Omega_{\rm m} = 0.3089$, $\Omega_\Lambda = 0.6911$, $\Omega_{\rm b} = 0.0486$, and $h = 0.6774$ (Planck Collaboration, 2016). We preform the following resolution-based cuts on this sample to best compare to other literature: $m_{\rm halo} \geq 1000 m_{\rm DM}$ for well resolved halos and assembly histories, $m_{\rm gas} \geq 4.53 \times 10^5\,{\rm M}_\odot$ and $m_* \geq 4.53 \times 10^7\,{\rm M}_\odot$, akin to at least 1 gas and 100 stellar particles in the hydrodynamic analogue respectively. A last cut on the sample is to carry out our analysis on central galaxies only, due to the fact that dark matter halo information is not directly outputted for satellites in the catalogs. The result is a sample of 5272 central galaxies.

3 Star formation models

In this section, we summarize the three star formation recipes compared in this work. We will cover the Kennicutt-Schmidt relation, an H2-based recipe after performing multiphase partitioning (the fiducial in the SAM), and the PRFM framework.

3.1 Kennicutt-Schmidt relation

The Kennicutt-Schmidt relation is a well known method used to measure a galaxy's global SFR through its gas content. The relation was first shown in Schmidt (1959) where the Milky Way's SFR was found to be proportional to the square of the volumetric gas density based on local gas observations. This can

be mathematically expressed as SFR $\propto \rho_{\rm gas}^2$. Kennicutt (1989) further constrains this relation as the star formation rate surface density as a function of gas surface density, expressed with the following formalism:

$$\Sigma_{\rm SFR} = N_{\rm KS}{\Sigma_{\rm gas}}^{\alpha_{\rm KS}} \tag{1}$$

Where $N_{\rm KS}$ is a normalization factor and is $\alpha_{\rm KS}$ the power law index. Kennicutt (1989) used observations of 15 spiral galaxies with Hα, HI, and CO (as proxy for H2) emission to obtain a fitted power law of $\alpha_{\rm KS} = 1.3 \pm 0.3$. For the purposes of this work, we utilize the updated values of $N_{\rm KS} = 1.1 \times 10^{-4}$ and $\alpha_{\rm KS} = 1.4$ as expressed in Table 1 of Somerville *et al.* (2015).

3.2 H2-based star formation with multiphase partitioning

The star formation recipe used in the SC SAM requires the use of two models: a multiphase partitioning framework (Gnedin & Kravtsov, 2011) and a surface density-based model (Bigiel *et al.*, 2008). They both depend on the existence of a thin, radial disk profile that can be expressed as a surface density:

$$\Sigma_{\rm disk} = \frac{m_{\rm disk}}{2\pi r_{\rm disk}^2} \tag{2}$$

Which applies both to our gas ($\Sigma_{\rm gas}$), stellar (Σ_*), and star formation rate ($\Sigma_{\rm SFR}$) surface densities. In the case of the gas, it follows an radial exponential profile. Under the methodology described in Gnedin & Kravtsov (2011), the total gas is first partitioned into HI and H2 components. The disk is first subdivided into radial annuli, and the H2 fraction is calculated per annulus using fitting functions dependent on gas phase metallicity and the background radiation field. The H2 gas mass of the disk is then calculated via a 5th order Runga-Kutta integration. The calculated SFR is based off a scaling relationship as presented in Bigiel *et al.* (2008), where above a critical density threshold, the star formation surface density is proportional to the H2 gas surface density ($\Sigma_{\rm SFR} \propto \Sigma_{\rm H2}$) akin to Kennicutt-Schmidt.

3.3 Pressure regulated feedback modulated star formation

The concept of pressure regulated, feedback modulated (PRFM) star formation is well summarized in Ostriker & Kim (2022) to which we refer the reader to for a thorough, in-depth understanding. The basis of this work is that the ISM state and structure is dependent on the feedback energy produced by young stars, which is coupled to the structure and state of the gas disk. Through this coupling, an estimate of disk-based star formation can be conducted, circumventing the the need for assumptions on multiphase gas partitioning as well as the tracking of those chemical species in simulations. PRFM is constrained on the TIGRESS numerical framework (Kim & Ostriker, 2017) on a suite of high-resolution disk galaxy simulations. The following description of the equations in the framework is a summary of what is presented in Hassan *et al.* (in review).

One assumption of PRFM is that the total pressure is in thermodynamic and dynamical equilibrium with the weight of the disk:

$$P_{\rm tot} = W_{\rm tot} = \Sigma W = W_{\rm dm} + W_{\rm gas} + W_* \tag{3}$$

The considered components are the gas, dark matter, and stellar weights. Note that the stellar component primarily consists of the stellar disk, but can also include the weight of the stellar bulge if its contribution is significant. We can work with our effective equation of state to describe the gas in the ISM via a pressure-density relation:

$$P_{\rm tot} = \rho_{\rm gas}\sigma_{\rm eff}^2 \tag{4}$$

Where $\rho_{\rm gas} = \Sigma_{\rm gas}/(2H_{\rm gas})$ and $H_{\rm gas}$ is the ISM disk height. Note that we assume that $H = H_{\rm gas} = H_*$ in the SAM due to lack of resolution-based elements and for simplicity. We can calculate H as a quadratic solution and W as given in Hassan *et al.* (in review):

$$H = \frac{2\sigma_{\rm eff}^2}{\pi G(\Sigma_{\rm gas}+\Sigma_*) + \left[(\pi G)^2(\Sigma_{\rm gas}+\Sigma_*)^2 + 8\zeta_{\rm dm}\Omega_{\rm dm}^2\sigma_{\rm eff}^2\right]^{\frac{1}{2}}} \tag{5}$$

$$W_{\rm tot} = \frac{\Sigma_{\rm gas}}{4}\left(\pi G(\Sigma_{\rm gas}+\Sigma_*) + \left[(\pi G)^2(\Sigma_{\rm gas}+\Sigma_*)^2 + 8\zeta_{\rm dm}\Omega_{\rm dm}^2\sigma_{\rm eff}^2\right]^{\frac{1}{2}}\right) \tag{6}$$

We define $\Omega_{\rm dm}^2 = 4\pi G\rho_{\rm dm}$ to describe the dark matter angular velocity that is based on the local dark matter density evaluated at the disk radius with an NFW profile (Navarro *et al.*, 1997). $\zeta_{\rm dm}$ is a numerical coefficient taken to be approximately $1/3$ (Ostriker & Shetty, 2011). In the presence of a significant stellar bulge, we can substitute $\Omega_{\rm dm}^2 \rightarrow \Omega_{\rm dm}^2 + \Omega_{\rm bulge}^2$ in the above equations and solve accordingly. For the purposes of this work, we define 'significant' to be when $r_{\rm bulge} \geq r_{\rm disk}$, the case where the bulge completely envelopes the disk. We assume that the stellar bulge is has a constant density distribution throughout the stellar disk of $\rho_{\rm bulge} = m_{\rm bulge}/(\frac{4}{3}\pi r_{\rm bulge}^2)$. We refer the reader to Appendix A for in-depth calculations of the bulge contribution.

Solving for H and W requires knowledge of $\sigma_{\rm eff}$, information that is not outright apparent due the unresolved nature of the SAM. We begin with a guess of $\sigma_{\rm eff} = 15\,{\rm km\,s^{-1}}$ and must iteratively solve for a value using root finding techniques until convergence. We can first solve for $\sigma_{\rm eff}$ via $P_{\rm tot} = W$ (provided that W is first calculated with our initial guess) using Eq. 33 from Hassan *et al.* (in review):

$$\sigma_{\rm eff} = 12\,{\rm km\,s^{-1}}\left(\frac{P_{\rm tot}}{10^4 k_{\rm B}\,{\rm cm^{-3}\,K}}\right)^{0.22} \tag{7}$$

Using the new value of the vertical velocity dispersion, we feed our updated value of $\sigma_{\rm eff}$ into Eq. 6 and our updated $W_{\rm tot}$ into Eq. 7 until convergence, to which we recalculate final values for H and $W_{\rm tot}$. We now can calculate the pressure-dependent feedback parameter $\Upsilon_{\rm tot}$:

$$\log_{10}(\Upsilon_{\rm tot}) = -0.212\log_{10}\left(\frac{P_{\rm tot}}{k_{\rm B}}\right) + 3.86 \tag{8}$$

Note that the feedback has units of ${\rm km\,s^{-1}}$. We now have all the information to solve for the relative ISM timescales being the (vertical) dynamical time ($t_{\rm dyn}$) and depletion time ($t_{\rm dep}$):

$$t_{\rm dyn} = \frac{2H_{\rm gas}}{\sigma_{\rm eff}} \tag{9}$$

$$t_{\rm dep} = \frac{\Upsilon_{\rm tot}}{\sigma_{\rm eff}} t_{\rm dyn} \tag{10}$$

We can last calculate our SFR using the depletion time of our gas as commonly done in simulations:

$$\dot{M}_* = \frac{m_{\rm gas}}{t_{\rm dep}} \tag{11}$$

4 Results

We outline the different properties analyzed to validate our model implementation. First, we ask how significant is a stellar bulge in the framework? Second, we carry out model validation by comparing our results to current and previous work. We last produce a predicted SFR utilizing the PRFM framework and compare the result to other models. We note that our PRFM-based predictions are done in post-processing, thus are not self-consistent.

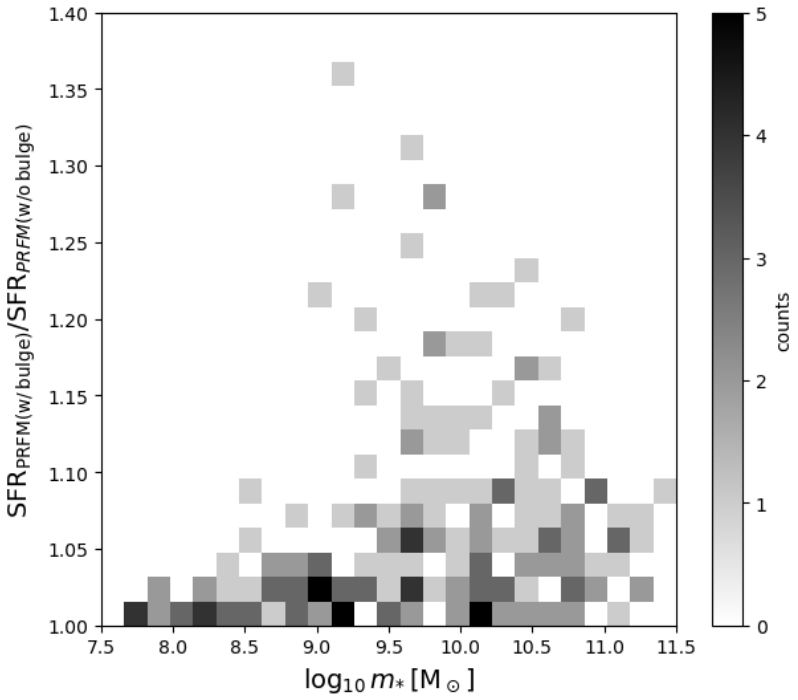

Figure 1: The ratio of calculated SFR using the PRFM framework when considering effects of with / without the stellar bulge mass as a function of galaxy stellar mass.

4.1 Impact of bulges on star formation in PRFM

We first investigate how much the contribution of a bulge affects the star formation rate in the PRFM framework. We identify 214 galaxies (approximately 4% of our sample) have what is considered a significant stellar bulge ($r_{\rm bulge} \geq r_{\rm disk}$). We note that this fraction can be considerably higher in larger, high-resolution cosmological boxes, further justifying the need for this comparison. We find that considering the stellar bulge in the PRFM framework increases galaxy star formation by a non-negligible amount, in some cases by up to $20 - 40\%$ as shown in Fig. 1. This, within the context of the model, makes sense. Increasing the weight directly increases the equilibrium pressure, which in turn decreases the feedback yield. A decrease in the feedback subsequently leads to a decrease in both the dynamical and depletion time of the gas, which last leads to an increase in star formation. There appears to be no strong correlation with this ratio as a function of galaxy stellar mass.

4.2 Model Validation

We next perform a series of model validations to confirm we are correctly producing the framework and results in post-processing as done in Hassan *et al.* (in review), where the post-processing was conducted on a sample of TNG50 galaxies from the hydrodynamic simulation analogue. Multiple studies have shown that $z = 0$ Santa Cruz SAM and TNG galaxy catalogs match fairly well (e.g. Gabrielpillai *et al.* (2022) for TNG100), thus providing us a natural comparison point when similarly post-processing.

The first comparison done is between the depletion time versus the vertical dynamical time of the gas as shown in the left of Fig. 2. A first observation is that the scatter from the original TIGRESS runs fits within the framework result's heatmap fairly well. There also appears to be a non-linear relationship between the depletion and dynamical time, which can potentially be captured a power law representation. The distribution of our results matches those seen in Hassan *et al.* (in review) fairly well, a first indication that our implementation of the framework has been implemented correctly in post-processing. The second

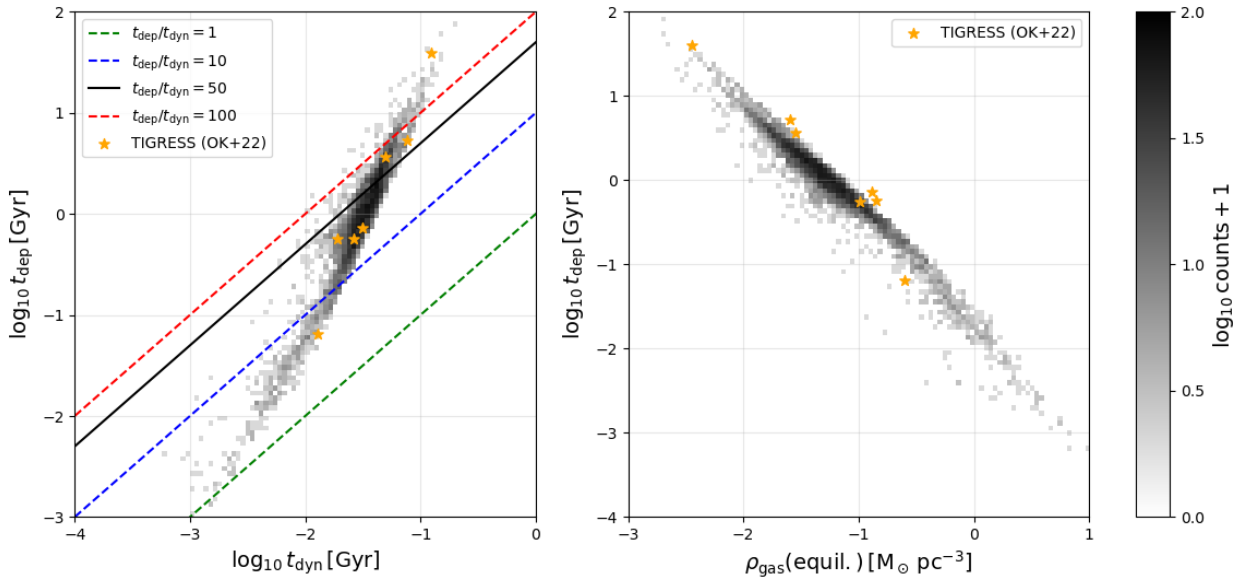

Figure 2: (Left) The depletion time vs. dynamical time of the ISM gas calculated using the PRFM framework. Overplotted in orange stars is data from TIGRESS simulation (Ostriker & Kim, 2022) and various slope parameters between the two timescales. (Right) The PRFM calculated depletion time vs. the equilibrium gas density calculated using the PRFM framework. Again overplotted are data points from the original TIGRESS suite (orange stars) used to constrain the framework.

comparison is relation between the depletion time and the equilibrium gas density, the right side of Fig. 2. The equilibrium gas density is given by $\rho_{\rm gas,equil.} = \Sigma_{\rm gas}/2H$, where (to reiterate) H is the solved-for disk gas height when in equilibrium. We again see that the TIGRESS data fits our scatter fairly well, and our results are again consistent with Hassan *et al.* (in review). We also observe that for galaxies with a low gas density that the depletion time is quite high as opposed to when the density is very high.

4.3 Model Comparisons

We last compare how our predicted SFR compares to the other star formation models. Figure 3 demonstrates this by plotting the star formation rate surface density against the gas surface density used. While the gas surface density in both PRFM and Kennicutt-Schmidt depends on the total ISM gas mass, the fiduical model is dependent only on the H2 component. We once again see that the PRFM framework reproduces the TIGRESS scatter quite well. When compared to the other models, if a power-law fit was conducted on the PRFM framework scatter, it appears that the power law index would be much higher than both the H2 partitioning and Kennicutt-Schmidt power laws. There is also a much wider scatter present in the framework results. Interestingly, PRFM predicts a much higher peak SFR surface density than the fiducial by almost two whole orders of magnitude, showing that PRFM has incredibly efficient star formation.

5 Discussion and Summary

5.1 Discussion

There are various assumptions we must reiterate regarding the PRFM framework and this work. First, the model was developed and tested using a simulation suite of disk dominated galaxies intended to describe the global behavior of star formation in the galactic disk. While there are considerations for specific case

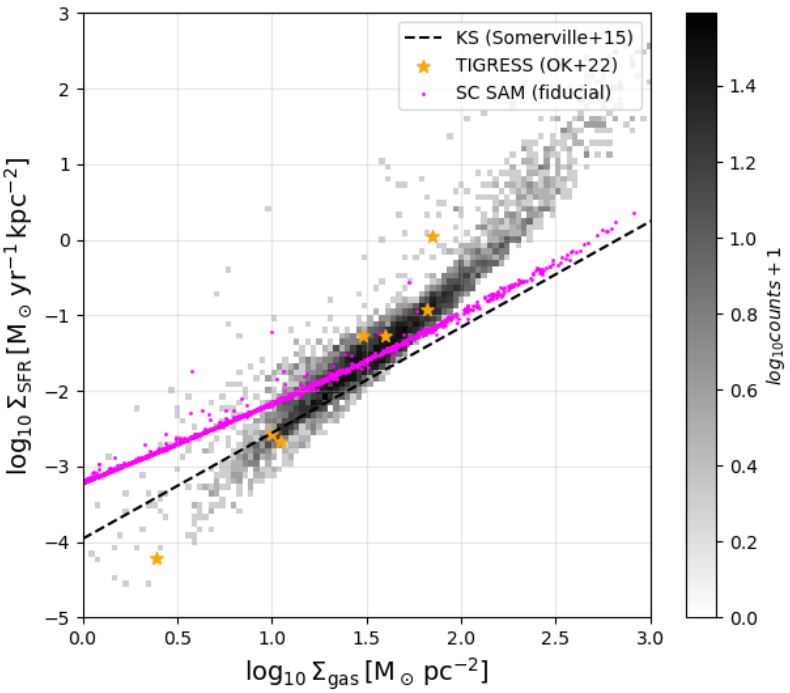

Figure 3: Star formation surface density calculated using the PRFM framework vs. gas surface density. TIGRESS galaxies are overplotted as orange stars. We also overplot the Kennicutt-Schmidt relation (dashed line) and the the fiducial SFR results outputted by the SAM (magenta dots).

scenarios (e.g. the presence of a significant stellar bulge), further testing is needed to see if the framework applies to as many possible galaxy types and environments, which is a computationally expensive problem.

Another important thing to note is that our process is not-self consistent and done in post-processing. A key part of this work was (i) making sure that we have the necessary information the SAM to utilize the framework, and (ii) outlining algorithms and methodology for implementing it. With this basis, we know now what needs to be done to add this star formation recipe in the SAM for self-consistent evolution. Before doing so, one more test is needed – the treatment of satellite galaxies. It is currently debated if satellites can even form stars when looking at results from surveys as SAGA (Geha *et al.*, 2017) and ELVES (Carlsten *et al.*, 2022), so careful consideration of their physics is required.

The lack of correlation between increase in star formation via stellar bulge mass contribution as a function of galaxy stellar mass (Fig. 1) may be due to the fact that our sample is not representative enough of bulge dominated galaxies, which are typically the product of multiple massive mergers. This check can be carried using catalogs from the other TNG volumes with side lengths of 100 and 300 Mpc. There is also the case to be made that bulge dominated galaxies can be considered as redder elliptical galaxies that do not have much star formation occurring to begin with. There are multiple avenues of investigation that can be taken to fully quantify and understand the effect the stellar bulge has on star formation in the framework.

There is strong potential for this framework answering the current question posited by recent JWST observations: why are very young galaxies apparently massive and bright? UV luminosity functions for $z > 9$ have a higher brighter end than originally expected. One possible solution is that star formation was incredibly bursty in the early universe. Another is that star formation was relatively incredibly efficient when compared to now. PRFM, shown to be an efficient star formation model, may be able to demonstrate the latter provided that $z = 0$ results are still fairly constrained by observations such as galactic SFRs and gas contents, which need to be used with care and appropriately.

5.2 Summary

As we have shown in this work, we are able to apply the PRFM framework for galactic star formation in post-processing on galaxy catalogs produced by the Santa Cruz SAM. We both reproduce the scatter in the TIGRESS simulations for a number of scaling relations and match what is expected when compared to other post-processed catalogs. We have set the groundwork for implementing this model in SAMs for self-consistent evolution, testing in large-scale environments, and seeing if we can naturally recover current JWST observations.

References

Behroozi, Peter S., Wechsler, Risa H., Wu, Hao-Yi, Busha, Michael T., Klypin, Anatoly A., & Primack, Joel R. 2013a. Gravitationally Consistent Halo Catalogs and Merger Trees for Precision Cosmology. , **763**(1), 18.

Behroozi, Peter S., Wechsler, Risa H., & Wu, Hao-Yi. 2013b. The ROCKSTAR Phase-space Temporal Halo Finder and the Velocity Offsets of Cluster Cores. , **762**(2), 109.

Bigiel, F., Leroy, A., Walter, F., Brinks, E., de Blok, W. J. G., Madore, B., & Thornley, M. D. 2008. The Star Formation Law in Nearby Galaxies on Sub-Kpc Scales. , **136**(6), 2846–2871.

Carlsten, Scott G., Greene, Jenny E., Beaton, Rachael L., Danieli, Shany, & Greco, Johnny P. 2022. The Exploration of Local VolumE Satellites (ELVES) Survey: A Nearly Volume-limited Sample of Nearby Dwarf Satellite Systems. , **933**(1), 47.

Gabrielpillai, Austen, Somerville, Rachel S., Genel, Shy, Rodriguez-Gomez, Vicente, Pandya, Viraj, Yung, L. Y. Aaron, & Hernquist, Lars. 2022. Galaxy formation in the Santa Cruz semi-analytic model compared with IllustrisTNG - I. Galaxy scaling relations, dispersions, and residuals at z = 0. , **517**(4), 6091–6111.

Geha, Marla, Wechsler, Risa H., Mao, Yao-Yuan, Tollerud, Erik J., Weiner, Benjamin, Bernstein, Rebecca, Hoyle, Ben, Marchi, Sebastian, Marshall, Phil J., Muñoz, Ricardo, & Lu, Yu. 2017. The SAGA Survey. I. Satellite Galaxy Populations around Eight Milky Way Analogs. , **847**(1), 4.

Gnedin, Nickolay Y., & Kravtsov, Andrey V. 2011. Environmental Dependence of the Kennicutt-Schmidt Relation in Galaxies. , **728**(2), 88.

Hassan, Sultan., Ostriker, Eve C., Kim, Chang-Goo, Bryan, Greg, Genel, Shy, Hernquist, Lars, ..., & Somerville, Rachel S. in review. Comparing Star Formation in TNG50 with the Pressure-Regulated, Feedback-Modulated Equilibrium Model. .

Kennicutt, Robert C., Jr. 1989. The Star Formation Law in Galactic Disks. , **344**(Sept.), 685.

Kim, Chang-Goo, & Ostriker, Eve C. 2017. Three-phase Interstellar Medium in Galaxies Resolving Evolution with Star Formation and Supernova Feedback (TIGRESS): Algorithms, Fiducial Model, and Convergence. , **846**(2), 133.

Navarro, Julio F., Frenk, Carlos S., & White, Simon D. M. 1997. A Universal Density Profile from Hierarchical Clustering. , **490**(2), 493–508.

Nelson, Dylan, Pillepich, Annalisa, Springel, Volker, Weinberger, Rainer, Hernquist, Lars, Pakmor, Rüdiger, Genel, Shy, Torrey, Paul, Vogelsberger, Mark, Kauffmann, Guinevere, Marinacci, Federico, & Naiman, Jill. 2018. First results from the IllustrisTNG simulations: the galaxy colour bimodality. , **475**(1), 624–647.

Nelson, Dylan, Pillepich, Annalisa, Springel, Volker, Pakmor, Rüdiger, Weinberger, Rainer, Genel, Shy, Torrey, Paul, Vogelsberger, Mark, Marinacci, Federico, & Hernquist, Lars. 2019. First results from the TNG50 simulation: galactic outflows driven by supernovae and black hole feedback. , **490**(3), 3234–3261.

Ostriker, Eve C., & Kim, Chang-Goo. 2022. Pressure-regulated, Feedback-modulated Star Formation in Disk Galaxies. , **936**(2), 137.

Ostriker, Eve C., & Shetty, Rahul. 2011. Maximally Star-forming Galactic Disks. I. Starburst Regulation Via Feedback-driven Turbulence. , **731**(1), 41.

Pillepich, Annalisa, Nelson, Dylan, Springel, Volker, Pakmor, Rüdiger, Torrey, Paul, Weinberger, Rainer, Vogelsberger, Mark, Marinacci, Federico, Genel, Shy, van der Wel, Arjen, & Hernquist, Lars. 2019. First results from the TNG50 simulation: the evolution of stellar and gaseous discs across cosmic time. , **490**(3), 3196–3233.

Planck Collaboration. 2016. Planck 2015 results. XIII. Cosmological parameters. , **594**(Sept.), A13.

Schmidt, Maarten. 1959. The Rate of Star Formation. , **129**(Mar.), 243.

Somerville, Rachel S., Popping, Gergö, & Trager, Scott C. 2015. Star formation in semi-analytic galaxy formation models with multiphase gas. , **453**(4), 4337–4367.

Somerville, Rachel S., Olsen, Charlotte, Yung, L. Y. Aaron, Pacifici, Camilla, Ferguson, Henry C., Behroozi, Peter, Osborne, Shannon, Wechsler, Risa H., Pandya, Viraj, Faber, Sandra M., Primack, Joel R., & Dekel, Avishai. 2021. Mock light-cones and theory friendly catalogues for the CANDELS survey. , **502**(4), 4858–4876.

A Solving for disk H and W with a significant stellar bulge

We can break down W_* into two components: a stellar disk ($W_{*,\,\mathrm{disk}}$) and stellar bulge ($W_{*,\,\mathrm{disk}}$). We assume that $H = H_{\mathrm{gas}} = H_*$ for simplicity in the SAM utilize Eqs. 8 and 9 from Hassan *et al.* (in review):

$$W_{*,\,\mathrm{disk}} \approx \pi G \Sigma_{\mathrm{gas}} \Sigma_* \frac{H_{\mathrm{gas}}}{H_{\mathrm{gas}} + H_*} = \frac{\pi G \Sigma_{\mathrm{gas}} \Sigma_*}{2} \tag{12}$$

$$W_{*,\,\mathrm{bulge}} = \int_0^{z_{\mathrm{max}}} \rho_{\mathrm{gas}} g_{*,\,\mathrm{bulge}} dz = \zeta_{\mathrm{d}} \Sigma_{\mathrm{gas}} \Omega^2_{*,\mathrm{bulge}} H \tag{13}$$

We can write our pressure-weight balancing expression as a sum of all the resolvable components that comprises the galaxy in our model, such as the gas, stars, and dark matter (Eq. 4, Hassan *et al.* (in review)):

$$P_{\mathrm{tot}} = \frac{\Sigma_{\mathrm{gas}}}{2H} \sigma^2_{\mathrm{eff}} = W_{\mathrm{gas}} + W_* + W_{\mathrm{dm}} = W_{\mathrm{gas}} + \Big[W_{*,\mathrm{disk}} + W_{*,\mathrm{bulge}} \Big] + W_{\mathrm{dm}} \tag{14}$$

$$\frac{\Sigma_{\mathrm{gas}}}{2H} \sigma^2_{\mathrm{eff}} = \frac{\pi G \Sigma^2_{\mathrm{gas}}}{2} + \frac{\pi G \Sigma_{\mathrm{gas}} \Sigma_*}{2} + \zeta_{\mathrm{d}} \Sigma_{\mathrm{gas}} \Omega^2_{*,\mathrm{bulge}} H + \zeta_{\mathrm{d}} \Sigma_{\mathrm{gas}} \Omega^2_{\mathrm{dm}} H \tag{15}$$

We note that the stellar bulge and dark matter weight contributions share similar expressions, thus we can combine them nicely as such:

$$\frac{\Sigma_{\mathrm{gas}}}{2H} \sigma^2_{\mathrm{eff}} = \frac{\pi G \Sigma^2_{\mathrm{gas}}}{2} + \frac{\pi G \Sigma_{\mathrm{gas}} \Sigma_*}{2} + \zeta_{\mathrm{d}} \Sigma_{\mathrm{gas}} \left(\Omega^2_{*,\mathrm{bulge}} + \Omega^2_{\mathrm{dm}} \right) H \tag{16}$$

$$\frac{\sigma^2_{\mathrm{eff}}}{H^2} = \frac{\pi G \Sigma_{\mathrm{gas}} + \pi G \Sigma_*}{H} + 2\zeta_{\mathrm{d}} \left(\Omega^2_{*,\mathrm{bulge}} + \Omega^2_{\mathrm{dm}} \right) \tag{17}$$

$$-\sigma^2_{\mathrm{eff}} \frac{1}{H^2} + \pi G \left(\Sigma_{\mathrm{gas}} + \Sigma_* \right) \frac{1}{H} + 2\zeta_{\mathrm{d}} \left(\Omega^2_{*,\mathrm{bulge}} + \Omega^2_{\mathrm{dm}} \right) = 0 \tag{18}$$

We can rearrange and express our equation as a quadratic solution by setting $x = 1/H$:

$$-\sigma^2_{\mathrm{eff}} x^2 + \pi G \left(\Sigma_{\mathrm{gas}} + \Sigma_* \right) x + 2\zeta_{\mathrm{d}} \left(\Omega^2_{*,\mathrm{bulge}} + \Omega^2_{\mathrm{dm}} \right) = 0 \tag{19}$$

We solve for x using quadratic formula, $x = \frac{-b \pm \sqrt{b^2 - 4ac}}{2a}$, where $a = -\sigma^2_{\mathrm{eff}}$, $b = \pi G \left(\Sigma_{\mathrm{gas}} + \Sigma_* \right)$, and $c = 2\zeta_{\mathrm{d}} \left(\Omega^2_{*,\mathrm{bulge}} + \Omega^2_{\mathrm{dm}} \right)$:

$$x = \frac{-\pi G \left(\Sigma_{\mathrm{gas}} + \Sigma_* \right) \pm \left[\left(\pi G \left(\Sigma_{\mathrm{gas}} + \Sigma_* \right) \right)^2 - 4(-\sigma^2_{\mathrm{eff}}) \left(2\zeta_{\mathrm{d}} \left(\Omega^2_{*,\mathrm{bulge}} + \Omega^2_{\mathrm{dm}} \right) \right) \right]^{1/2}}{2(-\sigma^2_{\mathrm{eff}})} \tag{20}$$

We re-express our expression above for H:

$$x = \frac{1}{H} = \frac{\pi G \left(\Sigma_{\mathrm{gas}} + \Sigma_* \right) \mp \left[\pi^2 G^2 \left(\Sigma_{\mathrm{gas}} + \Sigma_* \right)^2 + 8\sigma^2_{\mathrm{eff}} \zeta_{\mathrm{d}} \left(\Omega^2_{*,\mathrm{bulge}} + \Omega^2_{\mathrm{dm}} \right) \right]^{1/2}}{2\sigma^2_{\mathrm{eff}}} \tag{21}$$

Which provides us the solution for the disk height:

$$H = \frac{2\sigma^2_{\mathrm{eff}}}{\pi G \left(\Sigma_{\mathrm{gas}} + \Sigma_* \right) + \left[\pi^2 G^2 \left(\Sigma_{\mathrm{gas}} + \Sigma_* \right)^2 + 8\sigma^2_{\mathrm{eff}} \zeta_{\mathrm{d}} \left(\Omega^2_{*,\mathrm{bulge}} + \Omega^2_{\mathrm{dm}} \right) \right]^{1/2}} \tag{22}$$

Which can also be used to solve for total disk weight:

$$W_{\mathrm{tot}} = P_{\mathrm{tot}} = \frac{\Sigma_{\mathrm{gas}}}{2H} \sigma^2_{\mathrm{eff}} \tag{23}$$

We note that in the event that the stellar bulge contribution is negligible, we recover the formalism as expressed in Ostriker & Kim (2022) that leads to the solutions presented in Hassan *et al.* (in review).